



ORIGINAL PAPER

Aeromechanics Analyses of a Modern Lift-Offset Coaxial Rotor in High-Speed Forward Flight

Young-Min Kwon¹ · Jae-Sang Park¹ · Seong-Yong Wie² · Hee Jung Kang³ · Do-Hyung Kim²

Received: 26 February 2020 / Revised: 2 May 2020 / Accepted: 11 June 2020 / Published online: 2 July 2020
© The Korean Society for Aeronautical & Space Sciences 2020

Abstract

This study conducts an aeromechanics analysis of a modern lift-offset coaxial rotor in high-speed flight. A lift-offset coaxial rotor of the Sikorsky X2 technology demonstrator (X2TD) is considered for the present study. For the analyses of rotor performance, blade airloads, and hub vibratory loads, a rotorcraft comprehensive analysis code, CAMRAD II, is used. For the rotor performance analysis at a flight speed of up to 250 knots, which is the maximum level flight speed of X2TD in flight test, the present prediction of rotor power is compared well with the flight test data. For the blade section airload analysis at 250 knots, the impulses of the section lift forces are observed because of the aerodynamic interactions between the upper and lower rotors. The 4/rev hub vibratory loads are predicted, and its variation trend is moderately compared with the previous analysis results. Furthermore, the rotor vibration index increases significantly in high-speed flight with an increase in the flight speed, and this is well correlated with the previous rotorcraft comprehensive analysis result. This study shows that the present modeling and analysis techniques are appropriate to analyze the aeromechanics, including the performance, blade airloads, and hub vibratory loads of a modern lift-offset rotor in high-speed flight.

Keyword Compound helicopter · Lift-offset rotor · X2 technology demonstrator · Performance analysis · Blade airload analysis · Hub vibratory load analysis

Nomenclature

| | |
|--------------------|---|
| c | Blade chord length, ft |
| C_d | Drag coefficient of an airfoil |
| C_l | Lift coefficient of an airfoil |
| C_m | Pitching moment coefficient of an airfoil |
| D | Drag force, lb |
| D_{rotor} | Rotor drag, lb |
| D_{total} | Total drag, lb |
| F_{4P} | 4/rev hub vibratory force, lb |
| GW | Gross weight, lb |
| L | Lift force, lb |
| L/D_e | Effective lift-to-drag ratio of the rotor |
| LOS | Lift-offset |
| M | Mach number |

| | |
|------------------------|--|
| M_{4P} | 4/rev hub vibratory moment, lb ft |
| $M_{\text{Adv.Lmt}}$ | Maximum Mach number of advancing blade tip |
| M_{roll} | Hub rolling moment of a rotor, lb ft |
| N_b | Number of blades for a rotor |
| P | Rotor power, hp |
| P_{coaxial} | Coaxial rotor power, hp |
| P_i | Induced power, hp |
| P_{lower} | Power of the lower rotor, hp |
| P_o | Profile power, hp |
| P_p | Parasite power, hp |
| $P_{\text{propeller}}$ | Propeller power, hp |
| P_{upper} | Power of the upper rotor, hp |
| q | Dynamic pressure, lb/ft ² |
| r | Radial position of the rotor blade, ft |
| R | Radius of the rotor, ft |
| T | Thrust of a rotor, lb |
| V, V_∞ | Flight speed, ft/sec |
| VI | Vibration index |
| V_{tip} | Rotor tip speed, ft/sec |
| X | Wind-axis drag force of the rotor, lb |
| α | Angle of attack, deg |
| α_0 | Zero-lift angle of attack, deg |
| η | Propulsive efficiency |

✉ Jae-Sang Park
aerotor@cnu.ac.kr

¹ Department of Aerospace Engineering, Chungnam National University, Daejeon 34134, Korea

² Aeronautics Technology Research Division, Korea Aerospace Research Institute, Daejeon 34133, Korea

³ Optionally Piloted Personal Air Vehicle Team, Korea Aerospace Research Institute, Daejeon 34133, Korea

σ_{TW} Total solidity of the coaxial rotor
 ψ Azimuth angle, deg

1 Introduction

The next generation of rotorcrafts has been developed to archive the maximum flight speed to be above 230 knots, which is almost twice that of the conventional helicopter using a single main rotor. Therefore, compound helicopters using wings and auxiliary propulsions as well as rotors have received significant attention in the rotorcraft community. Among compound helicopters with various configurations, as shown in Fig. 1, the lift-offset compound helicopter using a rigid coaxial rotor and auxiliary propulsions is considered one of the best candidates for both excellent high-speed flight and hovering and vertical take-off/landing.

The lift-offset rotor uses a rigid coaxial rotor system with ABCTM (Advancing Blade Concept, [1]) developed by Sikorsky Aircraft. Most lifts of each rotor are produced by advancing blades of a lift-offset rotor using ABCTM (Fig. 2); thus, the lift-offset coaxial rotor does not suffer from a dynamic stall on the retreating side. In addition, since the trim for the rotor rolling moment is not required, more lift on the advancing side can be produced than a conventional helicopter. Consequently, aerodynamic efficiency, such as the rotor lift-to-drag ratio, may be improved. Finally, the auxiliary propulsions allow the lift-offset compound helicopter to fly at a higher-speed when the rotor rotation speed is reduced (slowed down) appropriately. Because of the unique characteristics of a lift-offset coaxial rotor, the center of the lift force of each rotor is shifted from the hub center to the advancing side of each rotor. Thus, the lift-offset (LOS) can be defined as the hub rolling moment of each rotor (M_{roll}) divided by its thrust (T), as given in Eq. (1):

$$LOS = \frac{M_{roll}}{TR}, \quad (1)$$

where R is the radius of the rotor.

The XH-59A helicopter (Fig. 1a) was developed as the first lift-offset compound helicopter using ABCTM by NASA, US Army, and Sikorsky Aircraft [1]. It had three blades for each rotor and used two turbojet engines for auxiliary propulsions. In the flight tests in the 1970s, the XH-59A helicopter recorded the maximum speed of 240 knots in level flight. Although the XH-59A helicopter successfully demonstrated an outstanding high-speed forward flight capability, there were serious problems such as significant vibration level in high-speed flight, high fuel consumption of the turbojet engines, lower than expected rotor efficiency, difficulty in reduction of rotor rotational speed, and so on [2]. In the early 2000s, the lift-offset coaxial rotor using ABCTM was



(a) XH-59A technology demonstrator



(b) X2 technology demonstrator (X2TD)



(c) S-97 Raider



(d) SB>1 Defiant



(e) Raider-X

Fig. 1 Compound helicopters using lift-offset rotor with ABCTM, **a** XH-59A technology demonstrator, **b** X2 technology demonstrator (X2TD), **c** S-97 Raider, **d** SB > 1 Defiant, and **e** Raider-X

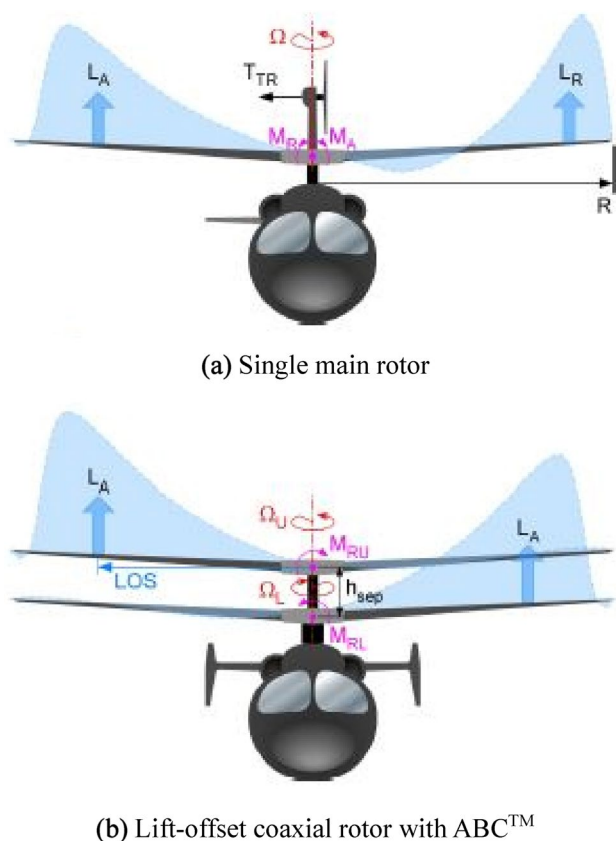


Fig. 2 Lift and rolling moment characteristics of conventional single rotor and lift-offset coaxial rotor [2]. **a** Single main rotor. **b** Lift-offset coaxial rotor with ABCTM

revisited through the X2 technology demonstrator (X2TD) program [3], since the advancement in technologies and improvement in design methodology, which had been developed over 20 years, could overcome the shortcomings of the previous XH-59A helicopter. These core technologies include fly-by-wire flight controls, all composite rigid rotor blades with an advanced aerodynamic blade design, more efficiently integrated rotor/auxiliary propulsion/engine control systems, active vibration control (AVC) systems, reduction of rotor rotational speed, and hub fairing with low drag. The X2TD achieved key performance parameters such as a cruise speed of 250 knots (recorded in a flight test in 2010), low pilot workload, low vibration, endurance of 5 h, and range radius of 110 nm [2]. Because of these excellent performances, the next generation of helicopters using the lift-offset coaxial rotor such as S-97 Raider, SB > 1 Defiant, and Raider-X (Fig. 1) has been developed based on the core technologies of the X2TD. Further detailed descriptions of the X2TD are given in the references [2–7].

Rotor aeromechanics analysis for performance, blade loads, vibration, and aeroelastic stability is very important when the rotorcrafts are developed. The CSD (computational

structural dynamics or rotorcraft comprehensive analysis)/CFD (computational fluid dynamics) coupled analysis is a state-of-the-art technique for the rotor aeromechanics predictions; however, it requires huge computational resources and time than the rotorcraft comprehensive analysis. A rotorcraft comprehensive analysis using the lifting-line theory, which is a lower order aerodynamics model, is quite useful, because it might provide relatively accurate predictions for rotor aeromechanics analysis with reasonable computational time, although it is not easy to capture the flow physics in detail, and various empirical parameters are required for the rotor aerodynamics and inflow/wake models. There have been intensive aeromechanics studies using the rotorcraft comprehensive analysis for the lift-offset compound helicopter. For the XH-59A helicopter, CAMRAD II [8] was used for the validation of performance [9, 10], and the correlation of performance, blade loads, and vibration with the flight test data [11]. CAMRAD II is an aeromechanics analysis code for performance, loads, vibration, and aeroelastic stability of rotorcrafts. It includes multibody dynamics, nonlinear finite elements, and rotorcraft aerodynamics based on the lifting-line theory along with various inflow/wake models. RCAS [12] was applied for trim optimization to minimize power and vibration at 250 knots [13], and to investigate the performance, loads, and vibration in different trim states [14]. RCAS is also a comprehensive analysis code for aerodynamics, performance, stability and control, aeroelastic stability, loads, and vibration of rotorcrafts. A hierarchical, finite-element, multibody dynamics formulation is employed for the structural dynamics model. RCAS has similar rotorcraft aerodynamics and inflow/wake models to CAMRAD II. For X2TD, not only the rotorcraft comprehensive analyses [9, 10, 15, 16] but also CSD/CFD coupled analyses [15–19] have been conducted recently. Since detailed data and information for the X2TD simulation modeling are not available in the public domain, the assumed or estimated properties were used for modeling the blade section properties, airfoils, and fuselage/propeller configurations in most works except the reference [19] by Sikorsky Aircraft. CAMRAD II with the freewake model was used to validate the X2TD performance [9, 10]. RCAS using the dynamic inflow model investigated the X2TD rotor performance and blade section airloads; however, the lift forces by fuselage and tail were not considered in the modeling [15]. In addition, the coupled analyses using RCAS/VVPM (Viscous Vortex Particle Method) and RCAS/CFD were conducted for blade airloads at a flight speed of 230 knots, and the prediction results were compared with the result by RCAS analysis using the dynamic inflow model [15]. The blade airloads and hub vibratory loads of the X2TD rotor at a flight speed of up to 150 knots were analyzed with an inhouse code (PrasadUM) using the freewake model developed at the University of Maryland [16]. The aerodynamic interaction of the X2TD

rotor in high-speed flight (at 200–225 knots) was investigated using the PrasadUM/Helios-coupled analysis [17]. The full X2 aircraft model, including the fuselage, pusher propeller as well as the lift-offset coaxial rotor, was used for the PrasadUM/Helios-coupled analysis to study the aerodynamic interactions between various components of the aircraft at 150 knots [18]. The RCAS/OVERFLOW-coupled analysis predicted the 4/rev hub vibratory loads of the X2TD rotor at the flight speed of 20–250 knots, and the results were compared with the flight test data [19]. However, the detailed modeling techniques of the X2TD rotor were not described, and the digits in the results were appropriately deleted.

As the X2TD is considered a modern and baseline model to develop the next generation of helicopters using the lift-offset coaxial rotor such as S-97 Raider, SB > 1 Defiant, and Raider-X [19], the techniques of modeling and aeromechanics analysis are important for the X2TD rotor. Although the previous works [9, 10, 15–19] were conducted intensely, there are limited works using the rotorcraft comprehensive analysis for the blade airloads and hub vibratory loads analyses at 250 knots, which is the maximum flight speed of the X2TD. Therefore, the present work using CAMRAD II investigates the aeromechanics including the performance, blade section airloads, and hub vibratory loads for the X2TD rotor at a flight speed of up to 250 knots.

2 Analytical Methods

2.1 Analytical Model

The general properties of X2TD are given in Table 1 [2, 16], and are compared with those of its predecessor, the XH-59A. The X2TD rotor uses an advanced blade design

for the planform, built-in twist, and airfoil to minimize the retreating blade drag losses. Figure 3 shows the geometric parameters of the X2TD main rotor [2]. The XH-59A rotor uses a trapezoidal planform, while the elliptical distribution of chord length in the main section is used for the X2TD rotor. In addition, the built-in twist distribution of the X2TD rotor is unique, since a positive value (14°) is used at $r/R=0.0-0.4$, but a negative value (-9°) is used at $r/R=0.4-1.0$. The blade dynamics characteristics of the X2TD rotor are found in the reference [4], and the flight test data for performance can be obtained from the reference [6]. Since the detailed properties or data for modeling of the X2TD are unavailable in the public domain, similar to the previous works [9, 10, 15–18], they are assumed appropriately for the present modeling and analysis of the X2TD rotor. Therefore, the rotor in this work should be defined as the notional X2TD rotor or X2TD-like rotor, for simplicity, but is called as the X2TD rotor.

2.2 Modeling and Analysis Techniques

Since the airfoils of the X2TD rotor blade are not available in the public domain, similar to the modeling technique in the reference [15], it is assumed that the airfoil section consists of DBLN526, SC325218, SC36212, SC36210, and SSCA09 airfoils, as shown in Fig. 4. The airfoil coordinates can be obtained from the reference [20]. MSES [21], a boundary layer-coupled Euler code, is used to generate the airfoil database (airfoil tables) including the lift (c_l), drag (c_d), and pitching moment (c_m) coefficients of an airfoil at various Mach numbers (M) and angles of attack (α). The aerodynamic coefficients (c_l , c_d , and c_m) of an airfoil in the region of high angle of attack are estimated using the following equations [22]:

Table 1 General properties of the XH-59A and X2TD aircrafts [2, 16]

| | XH-59A | X2TD |
|--|--|----------------------------|
| Gross weight, GW, (lb) | 13,300 | 5955 |
| Radius, R , (ft) | 18.0 | 13.2 |
| Number of rotors | 2 | 2 |
| Number of blades per rotor, N_b | 3 | 4 |
| Total solidity, σ_{TW} | 0.1275 | 0.1441 |
| Hub type | Rigid coaxial rotor | |
| Rotation direction | Upper rotor CCW Lower rotor CW | |
| Nominal rotor tip speed, V_{tip} , (ft/sec) | 650.0 | 620.45 |
| Advancing blade tip Mach number, $M_{Adv.Lmt}$ | 0.85 | 0.90 |
| Rotor vertical separation (ft) | 2.5 | 1.5 |
| Power plant (s) | 2 P&W J60-P-3A 1 P&W PT6T-3 Twin Pack | LHTEC T800-LHT- T801 |
| Maximum level flight speed (knots) | 240 | 250 |

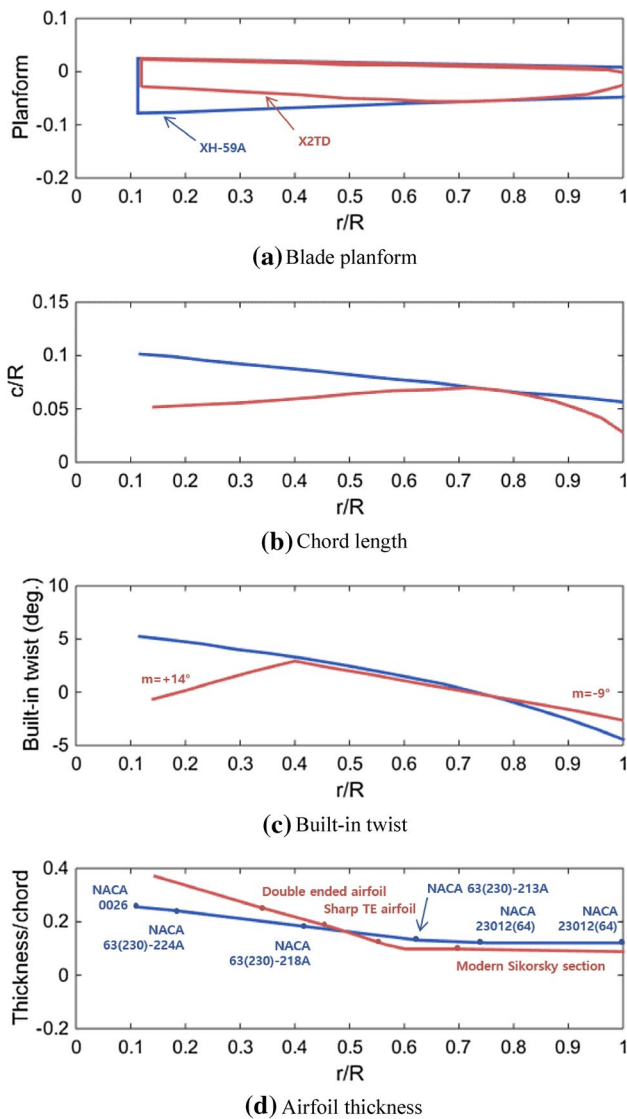


Fig. 3 Geometric parameters of X2TD main rotor [2]. **a** Blade planform, **b** Chord length, **c** Built-in twist, and **d** Airfoil thickness

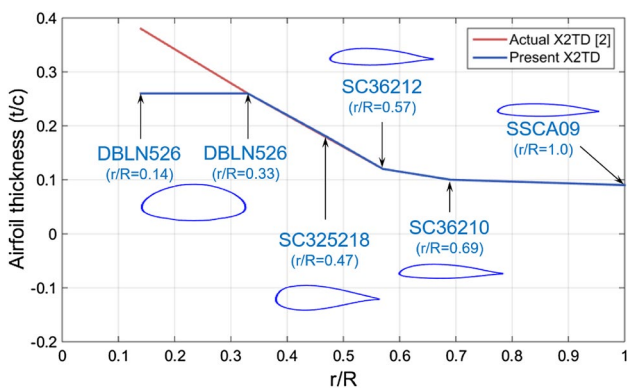


Fig. 4 Airfoil section distribution

$$c_l = A \sin 2(\alpha - \alpha_0), \tag{2a}$$

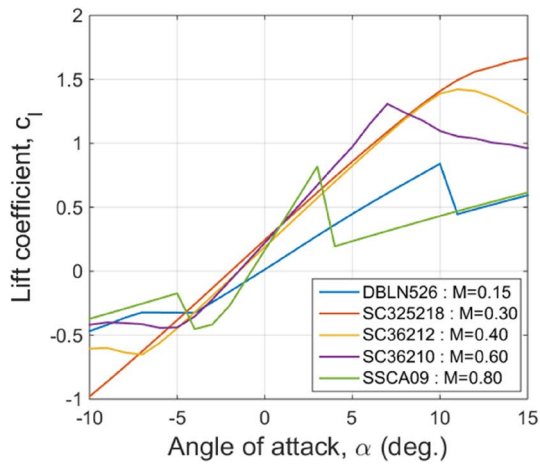
$$c_d = D + E \cos 2(\alpha - \alpha_0), \tag{2b}$$

$$c_m = B \sin (\alpha - \alpha_0) + C \sin 2(\alpha - \alpha_0), \tag{2c}$$

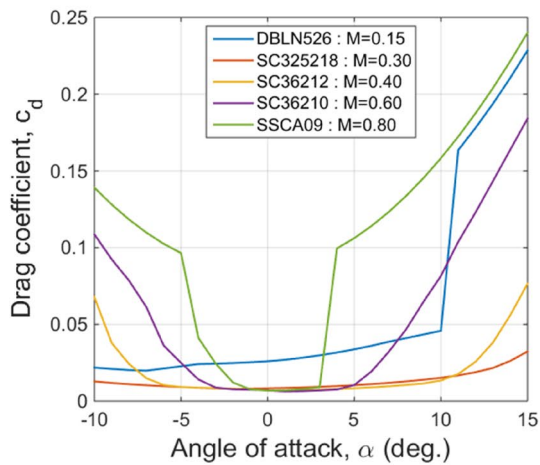
where α_0 is the zero-lift angle of attack. In addition, the values of $A, B, C, D,$ and E are assumed appropriately. The obtained aerodynamic coefficients of an airfoil are tabulated in the form of the standard airfoil table used in CAMRAD II modeling [8]. Examples of the calculated aerodynamic coefficients of the X2TD rotor airfoils in this study are shown in Fig. 5.

The aeromechanics of the X2TD rotor is investigated using a rotorcraft comprehensive analysis code, CAMRAD II. The present analysis model is based on the authors' previous work [11] for the analyses of the XH-59A lift-offset compound helicopter. Figure 6 shows the CAMRAD II model for the X2TD rotor with a cross-over angle of 0° . The unsteady aerodynamics model in CAMRAD II is based on the second-order lifting-line theory. The aerodynamic loads on a rotor blade are calculated using 25 aerodynamic panels, and the panel's width is 6.3% R at the root and 2.6% R at the tip. The blade section aerodynamic forces and moments on each aerodynamic panel are calculated using the local angle of attack, Mach number at the $3c/4$ point, and aerodynamic coefficients from the airfoil tables previously generated using MSES. For airfoil table look-up, the Reynolds number correction method [23] is applied. The general free-wake model is used to consider the aerodynamic interaction between the upper and lower rotors. The rotor blade structural dynamics is modeled based on the nonlinear elastic beam theory considering small strain and moderate deflections. In this work, seven nonlinear finite beam elements are used for a blade. Each finite beam element has 15 degrees of freedom with four flap, four lead-lag, three torsion, and four axial nodal variables. The blade section properties in the present modeling are obtained from Mach-scaled XH-59A blade section properties, and they are slightly modified, similar to the previous works [9, 10, 15–18]. In addition, a rotor control system, which includes the pitch link, swash-plates, and pitch horn, is also modeled. The pitch-link stiffness value is assumed appropriately to match the nonrotating blade natural frequency in the first torsion mode given from the reference [4].

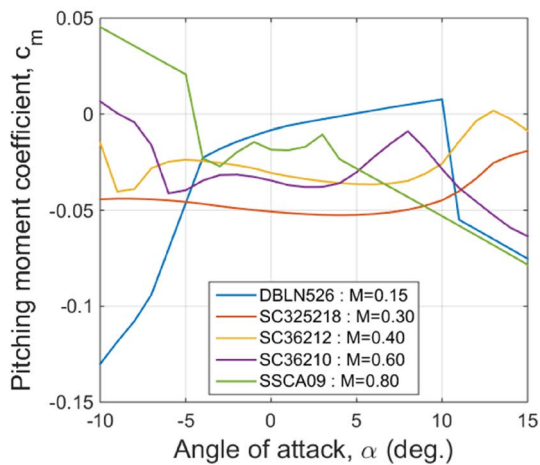
For the CAMRAD II modeling, the rotor rotational speed is scheduled in order not to exceed the advancing tip Mach number to 0.9, as shown in Fig. 7. Figure 8 shows scheduled the lateral lift-offset based on the measured data [6]. This study uses an isolated rotor model, rather than the completed X2TD model. Thus, similar to the approach used in the references [9, 10], the rotor shaft angle (Fig. 9) is assumed, so



(a) Lift coefficient



(b) Drag coefficient



(c) Pitching moment coefficient

Fig. 5 Examples of calculated aerodynamic coefficients of X2TD rotor airfoils. **a** Lift coefficient, **b** Drag coefficient, and **c** Pitching moment coefficient

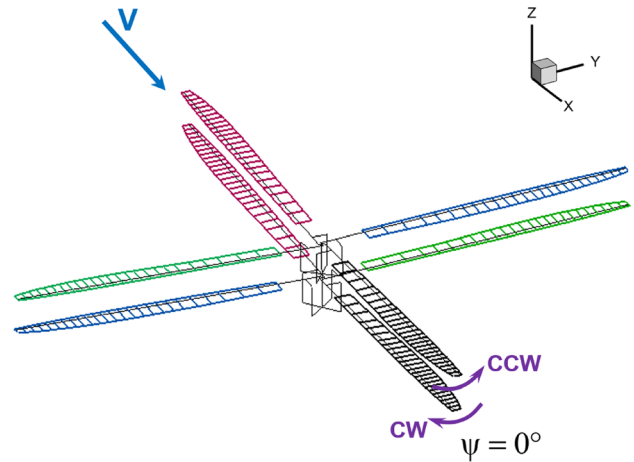


Fig. 6 CAMRAD II model of X2TD rotor (cross-over angle = 0°)

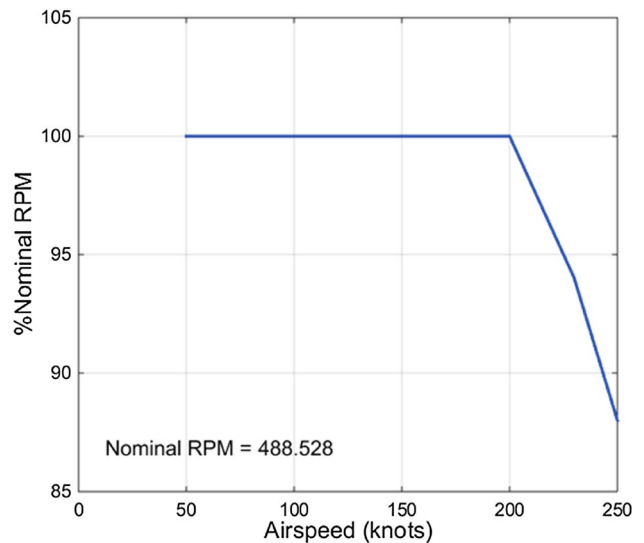


Fig. 7 Rotor rotational speed schedule

that the calculated rotor power (at 4000 ft and international standard atmosphere condition) can be matched to the flight test data [6]. The aircraft pitch angle in the X2TD flight test [6] was 2° – 5° , and the measured rotor power was nearly 0 above 150 knots. Most of the power was used to drive the pusher propeller for the propulsive force to overcome the rotorcraft’s drag at high-speed flight conditions. In addition, the propeller power, $P_{propeller}$, is also estimated using the following equations from the references [9, 10]:

$$P_{propeller} = \frac{D_{total} V}{\eta}, \tag{3a}$$

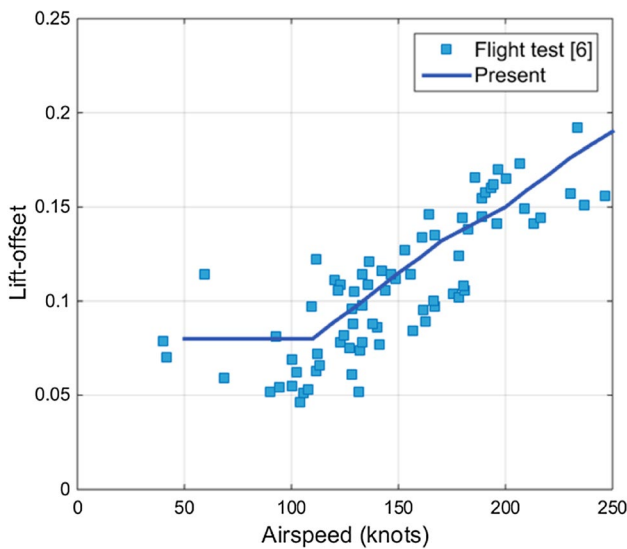


Fig. 8 Lateral lift-offset schedule

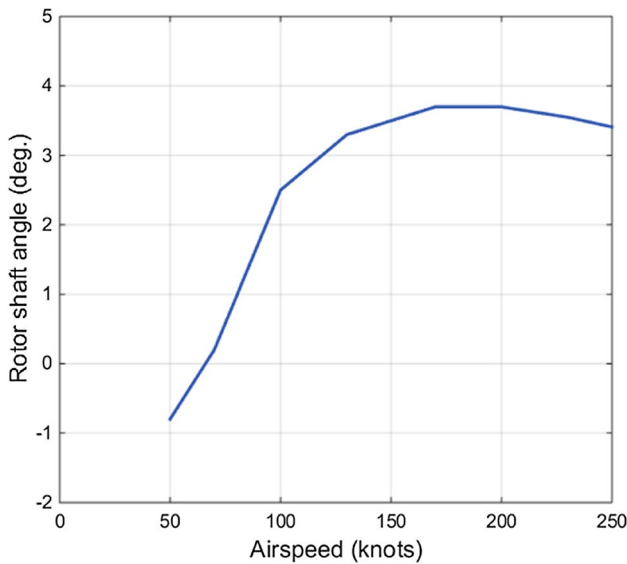


Fig. 9 Assumed rotor shaft angle

$$D_{total} = D_{rotor} + D_{airframe} = D_{rotor} + q \left(\frac{D}{q} \right)_{airframe}, \quad (3b)$$

$$\left(\frac{D}{q} \right)_{airframe} = 1.4 \left(\frac{GW}{1000} \right)^{2/3}, \quad (3c)$$

where D is the drag force, V is the flight speed, η is the propulsive efficiency (assumed to be 0.85 in this study), and q is the dynamic pressure. In addition, the rotor drag, D_{rotor} , is calculated by CAMRAD II analysis.

The six primary rotor controls of the upper and lower rotors are used to trim the rotor at the assumed rotor shaft pitch angle (given in Fig. 9). The rotor thrust is trimmed to the aircraft weight, excluding the lift by the fuselage and tail given in Fig. 10 [9]. The hub pitch moment of each rotor is trimmed to zero, and the torque offset of the upper and lower rotors is set to zero. In addition, the hub roll moment of each rotor is trimmed to the values prescribed using Eq. (1) with the given lift-offset value in Fig. 8. An azimuthal step of 15° is used to obtain the trim solution; however, the refined azimuthal resolution of 3.6° is considered for the blade section airload analysis using the post-trim method (this will be discussed in Sect. 3.3) to consider the aerodynamic interaction of the lift-offset coaxial rotor. This resolution is quite similar to the value of 3.75° used in the previous CSD analysis of the X2TD [16].

The power (P) of each rotor is calculated as:

$$P = P_i + P_o + P_p, \quad (4)$$

where P_i , P_o , and P_p are the induced power, profile power, and parasite power, respectively. In addition, the power of a lift-offset coaxial rotor, $P_{coaxial}$, is defined as the sum of each power of the upper and lower rotors as follows:

$$P_{coaxial} = P_{upper} + P_{lower}. \quad (5)$$

The rotor aerodynamic efficiency parameter, the effective lift-to-drag ratio of the rotor (L/D_e), is given as:

$$\frac{L}{D_e} = \frac{L}{P_{coaxial}/V + X}, \quad (6)$$

where X is the wind axis drag force of the rotor.

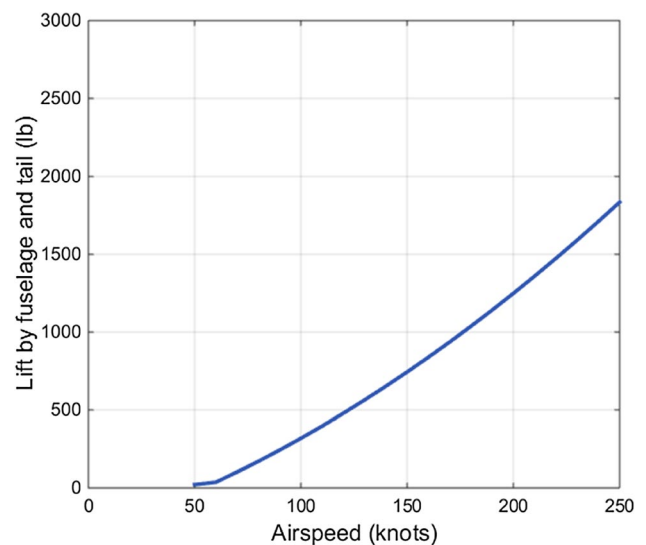


Fig. 10 Lift by fuselage and tail [9]

The 4/rev (4P) hub vibratory loads of the X2TD rotor are calculated using the following equations:

$$F_{4P} = \sqrt{\left(F_{4P_C}^{\text{upper}} + F_{4P_C}^{\text{lower}}\right)^2 + \left(F_{4P_S}^{\text{upper}} + F_{4P_S}^{\text{lower}}\right)^2}, \quad (7a)$$

$$M_{4P} = \sqrt{\left(M_{4P_C}^{\text{upper}} + M_{4P_C}^{\text{lower}}\right)^2 + \left(M_{4P_S}^{\text{upper}} + M_{4P_S}^{\text{lower}}\right)^2}, \quad (7b)$$

where F and M are the hub forces and moments, respectively. Furthermore, the subscripts, C and S , denote the cosine and sine components of the hub loads, respectively.

The rotor vibration level is evaluated using the vibration index (VI, [24]) which is expressed as:

$$VI = \frac{\sqrt{\left(0.5F_{x_{4P}}\right)^2 + \left(0.67F_{y_{4P}}\right)^2 + F_{z_{4P}}^2}}{GW} + \frac{\sqrt{M_{x_{4P}}^2 + M_{y_{4P}}^2}}{(R)(GW)}. \quad (8)$$

The interrotor cancellation of the lift-offset coaxial rotor [25] is considered when calculating the rotor vibration index in this study, and the 4/rev components are only used, because they are the most dominant for the X2TD rotor vibration.

3 Results and Discussion

3.1 Rotating Blade Frequency

The natural frequencies of a rotating blade for the X2TD rotor are calculated in Fig. 11 and compared with the previous predictions by Sikorsky Aircraft [4]. At the rotor rotational speed in hover, the discrepancies between the present calculations and previous predictions [4] in the first flap, lead-lag, torsion, and second flap modes (1F, 1L, 1T, and 2F, respectively) are -1.32 , 5.56 , -0.60 , and -6.12% , respectively. Therefore, the rotating blade natural frequencies in the first flap and torsion modes (1F and 1T, respectively) are well matched with the reference data [4]. The natural frequencies in the first lead-lag and second flap modes (1L and 2F, respectively) are also moderately predicted. However, the validations of the third flap (3F) and second lead-lag (2L) mode frequencies are not good, because the order of the two modes is exchanged, when compared with the previous work [4]. This correlation trend for the 3F and 2L modes is commonly observed from the previous works [9, 15, 16]. The modeling of the blade section properties will be improved for a better prediction of the X2TD rotor blade structural dynamics.

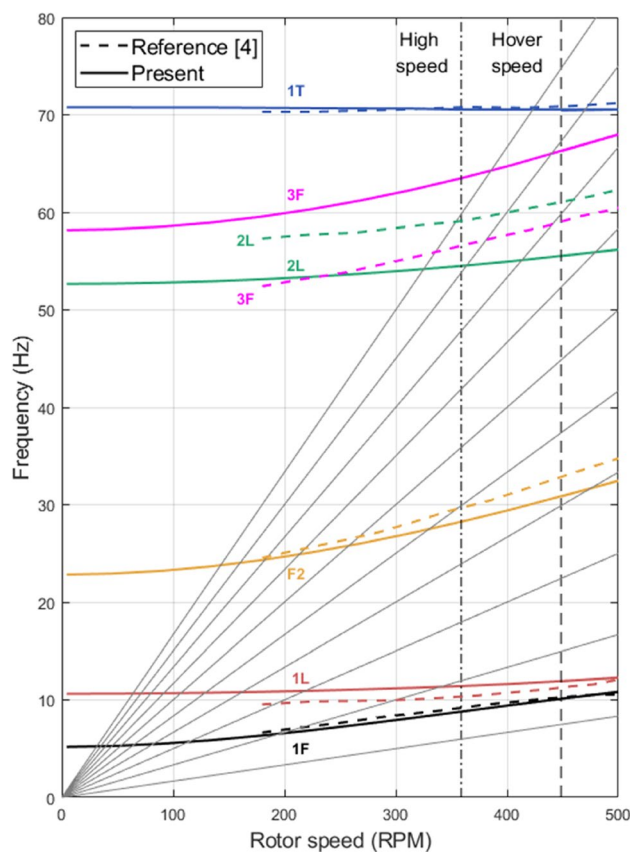


Fig. 11 Validation of fan plot analysis (collective pitch angle = 10°)

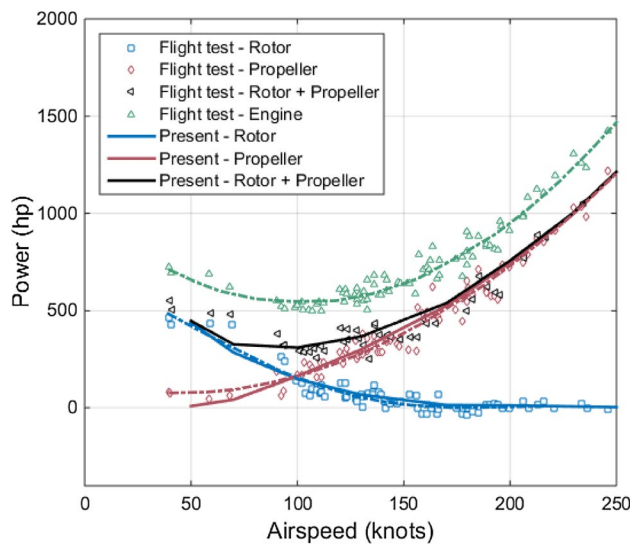


Fig. 12 Validation of power

3.2 Rotor Performance

Figure 12 validates the predicted power with the flight test data [6]. In the figure, the symbols represent the measured data from the X2TD flight tests, the dashed lines are for the curve-fitted flight test data, and the solid lines stand for the present predictions. The rotor power is excellently correlated with the measured data, and it decreases with an increase in the flight speed. The power of a pusher propeller is also well validated with the flight test result. As the flight speed increases, the propeller power increases significantly. Therefore, most power is used for the propeller in high-speed flight, while the rotor power is nearly zero. In addition, the sum of the rotor and propeller powers is compared nicely with the flight test data. As seen from this validation, the present modeling and analysis techniques can be considered appropriate for the X2TD rotor.

The rotor effective lift-to-drag ratio (L/D_e) is compared with the previous analysis result [10] in Fig. 13. At low speed to the maximum flight speed, the present prediction shows a good correlation with the previous analysis [10] in terms of both the maximum value and variation trend. Furthermore, the maximum value of L/D_e is higher than that of the XH-59A rotor [1]. This is because advanced airfoils and innovated blade design are used for the X2TD rotor [2].

Figure 14 shows the variations in the predicted lift and drag forces of the X2TD. As shown in Fig. 14a, the rotor lift decreases, but the lift by fuselage and tail (previously given in Fig. 10) increases with an increase in the flight speed. In addition, the lift force magnitudes of the upper and lower rotors are almost identical. The rotor drag force increases as the flight speed increases up to 150 knots, and then, it is nearly constant in high-speed flight; however, the airframe drag force [predicted by Eqs. (3b) and (3c)] increases

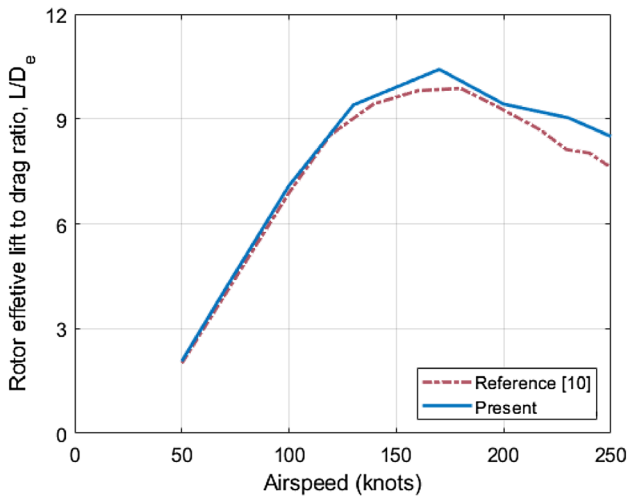


Fig. 13 Validation of rotor effective lift-to-drag ratio

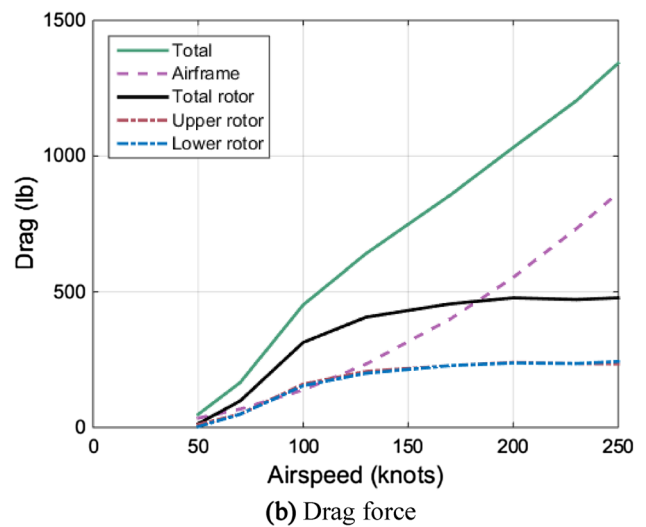
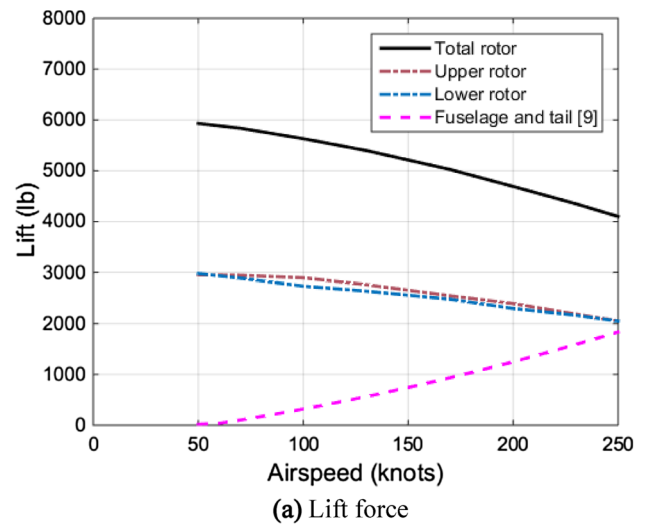


Fig. 14 Lift and drag forces. a Lift force, b Drag force

monotonically with the increase in airspeed, as shown in Fig. 14b. Furthermore, the magnitudes of drag force for both rotor are quite similar to each other.

3.3 Blade Section Airloads

In this section, the blade section airloads (lift, drag forces, and pitching moment) of the upper and lower rotors are predicted for the X2TD rotor at a flight speed of 250 knots (advance ratio μ of 0.773). All the section airloads are expressed in a nondimensional form with the local Mach number (M) and sectional aerodynamic coefficients (C_l , C_d , and C_m). The X2TD flight test did not measure the blade airloads, and there have not been the previous analysis works to predict the blade section airloads of the X2TD rotor at 250 knots. Therefore, the validation or correlation of the present results is not given in this section.

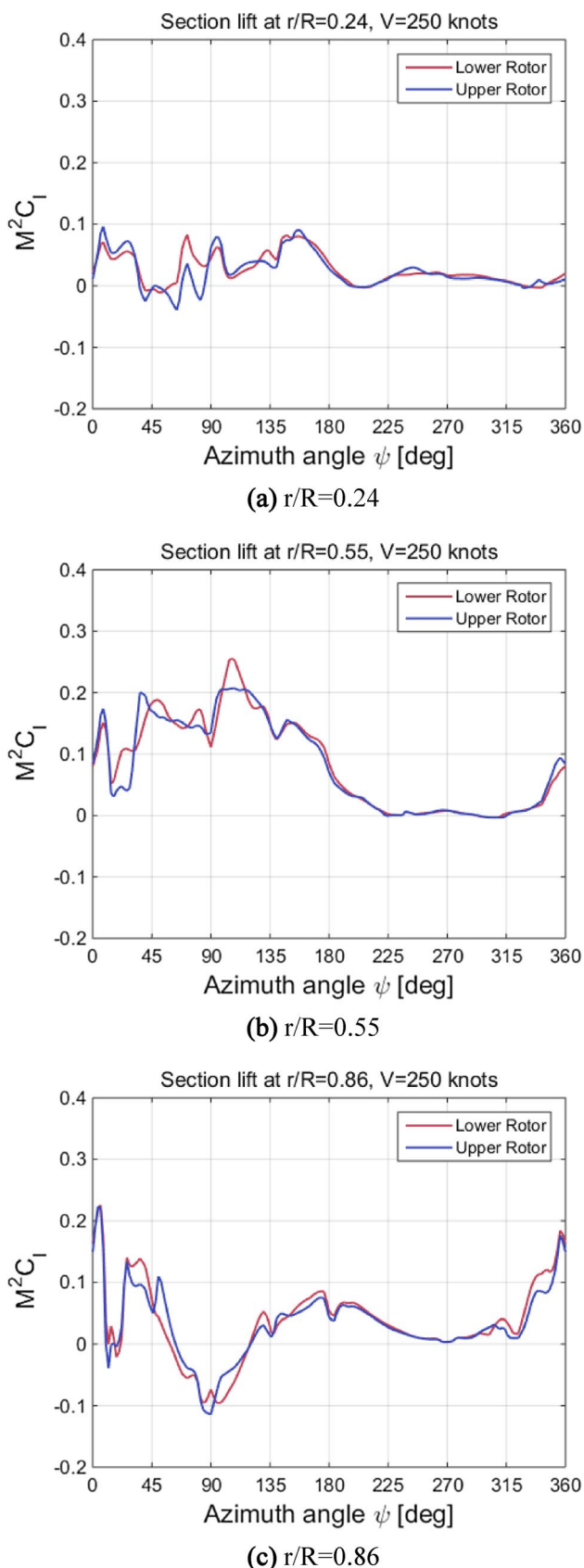


Fig. 15 Blade section lift forces (M^2C_l) at $V=250$ knots. **a** $r/R=0.24$, **b** $r/R=0.55$, **c** $r/R=0.86$

The section lift forces (M^2C_l) at three blade span locations ($r/R=0.24, 0.55$, and 0.86) of the upper and lower rotors at 250 knots are shown in Fig. 15. The azimuthal angle (ψ) in the figure is defined in the direction of each rotor rotation. At the blade inboard location ($r/R=0.24$), the section lift force of each rotor definitely fluctuates on the advancing side ($0^\circ \leq \psi \leq 180^\circ$), and a reverse-flow region is observed on the retreating side ($180^\circ \leq \psi \leq 360^\circ$). In addition, the M^2C_l variations of both rotors are quite similar to each other for one rotor revolution. At the mid-board location ($r/R=0.55$), eight aerodynamic interactions of each rotor are possible at 45° intervals ($\Delta\psi=45^\circ$); however, only four impulses of M^2C_l on the advancing side are observed in this prediction, and the others on the retreating side are not shown. Furthermore, the section lift force of each rotor is almost zero on the retreating side because of the unique characteristics of a lift-offset rotor using ABCTM, and the variations in M^2C_l for the upper and lower rotors are similar to each other. At the outboard position ($r/R=0.86$), the distinct characteristics of the section lift force are clearly observed for both rotors. Similar to the previous result at $r/R=0.55$, the eight M^2C_l impulses at $r/R=0.86$ of each rotor may exist for one rotor revolution, and the present analysis captures well these aerodynamic interactions of M^2C_l for both rotors, except one event at $\psi=225^\circ$. In addition, BVI (blade–vortex interaction) phenomenon along with the oscillations of M^2C_l of each rotor is predicted at $\psi=0^\circ-45^\circ$, and the negative lift is shown at around $\psi=90^\circ$. The retreating blade of each rotor is off-loaded nearly; this is a unique feature of the lift-offset rotor. Figures 16, 17, 18 show the contour plots of predicted M^2C_l , M^2C_d , and M^2C_m distributions for the upper and lower rotors of the X2TD at 250 knots. In these figures, the distributions of the section aerodynamic loads (M^2C_l , M^2C_d , and M^2C_m) of the upper and lower rotors are symmetric. As shown in Fig. 16, most of the lift force (M^2C_l) is generated on the advancing side of each rotor because of the application of ABCTM. In addition, most of the lift on the fore and aft regions of each rotor disk is outward from mid-span, and the negative loading in the blade outboard region is shown on each rotor disk. The reverse-flow region is definitely observed on the retreating side of each rotor disk. The distributions of the drag forces (M^2C_d) of the upper and lower rotors are plotted in Fig. 17. On the retreating side of each rotor, a high drag force in the blade inboard region because of the reverse flow is shown, and the highest drag force at the blade tip is on the advancing side of each rotor because of the compressibility effect. Figure 18 shows the pitching moment (M^2C_m) distributions of both rotors. The positive pitching moment (nose-up pitching moment) in the blade inboard region on the retreating side of each rotor is predicted because of

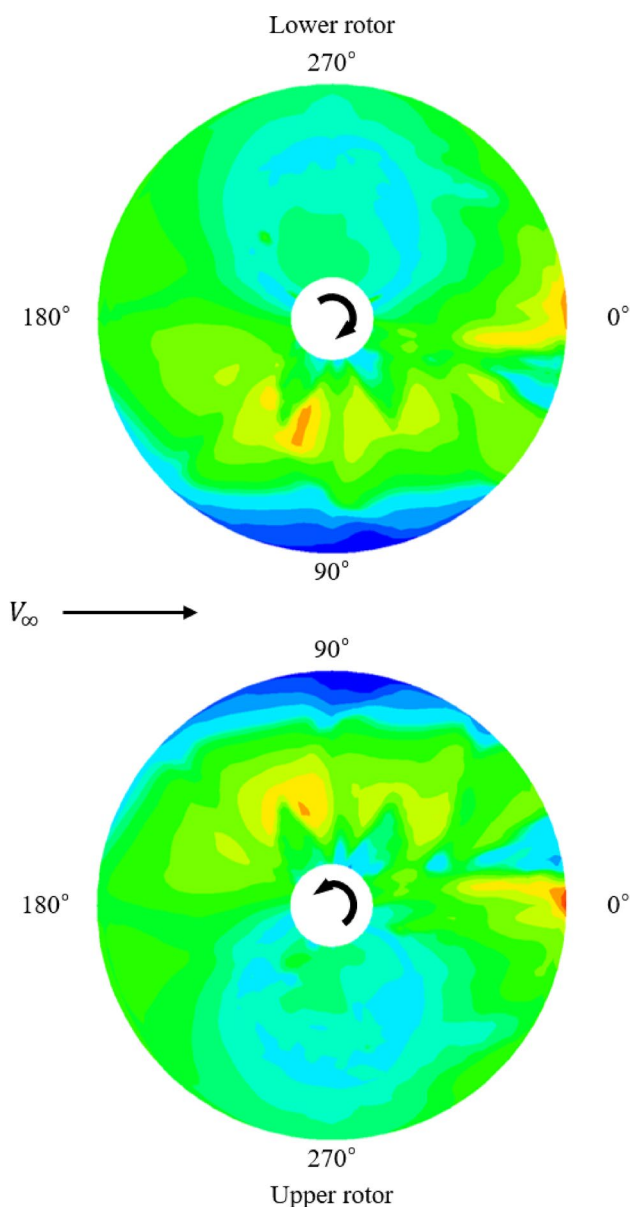


Fig. 16 Rotor lift force ($M^2 C_l$) distributions ($V=250$ knots)

the reverse flow; however, the pitching moment on each advancing side is negative (nose-down pitching moment).

3.4 Hub Vibratory Loads

In this section, the 4/rev (4P) hub vibratory loads of the X2TD rotor are investigated at a flight speed of up to 250 knots. Figures 19a and b compare the present 4/rev hub pitch moment (M_y) with the previous analyses and flight test data [19]. The 4P hub pitch moment is the most dominant component to the airframe vibration of the X2TD with a cross-over angle of 0° [6, 19], and the present 4/rev hub pitch moment (Fig. 19a) increases dramatically in high-speed flight (above

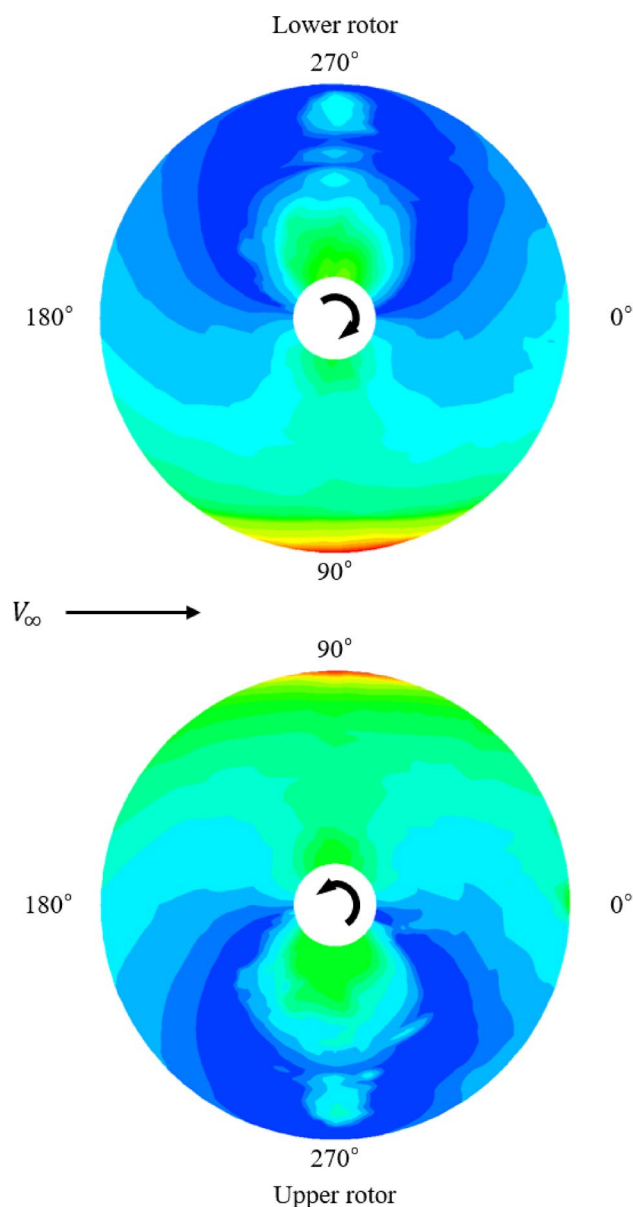


Fig. 17 Rotor drag force ($M^2 C_d$) distributions ($V=250$ knots)

150 knots) as the flight speed increases. The replotted results of the 4/rev hub pitch moment originally given in the reference [19] are shown in Fig. 19b. As can be seen, the present analysis using CAMRAD II is reasonably compared with the prediction by RCAS/OVERFLOW-coupled analysis [19] in terms of the variation trend; however, its magnitude is not validated, because the digits in the vertical axis are deleted originally in the reference [19]. In addition, the RCAS/OVERFLOW-coupled analysis overpredicts the 4/rev hub pitch moment at above 230 knots, when compared with the flight test data [19]. The 4/rev hub vertical force (F_{z4P}) and axial force (F_{x4P}) in the present analysis are shown in Figs. 19c and d, respectively. Two components of the 4/rev

hub vibratory loads both increase in the high-speed region as the airspeed increases. Figure 20 shows the vibration index [VI, calculated using Eq. (8)] of the X2TD rotor with an increase in the flight speed. As given in the figure, the rotor vibration index increases significantly in high-speed flight. Therefore, it is expected that there might be a serious vibration problem of the X2TD in high-speed flight test unless active vibration control (AVC) was applied to the airframe [4, 6]. In the present analysis, the variation trend of VI is quite similar to that of the 4/rev hub vertical force previously shown in Fig. 19c, and moderately resembles that of the 4/rev hub pitch moment in Fig. 19a. Furthermore, the present vibration index predicted by CAMRAD II is reasonably well compared to the previous PrasadUM analysis with

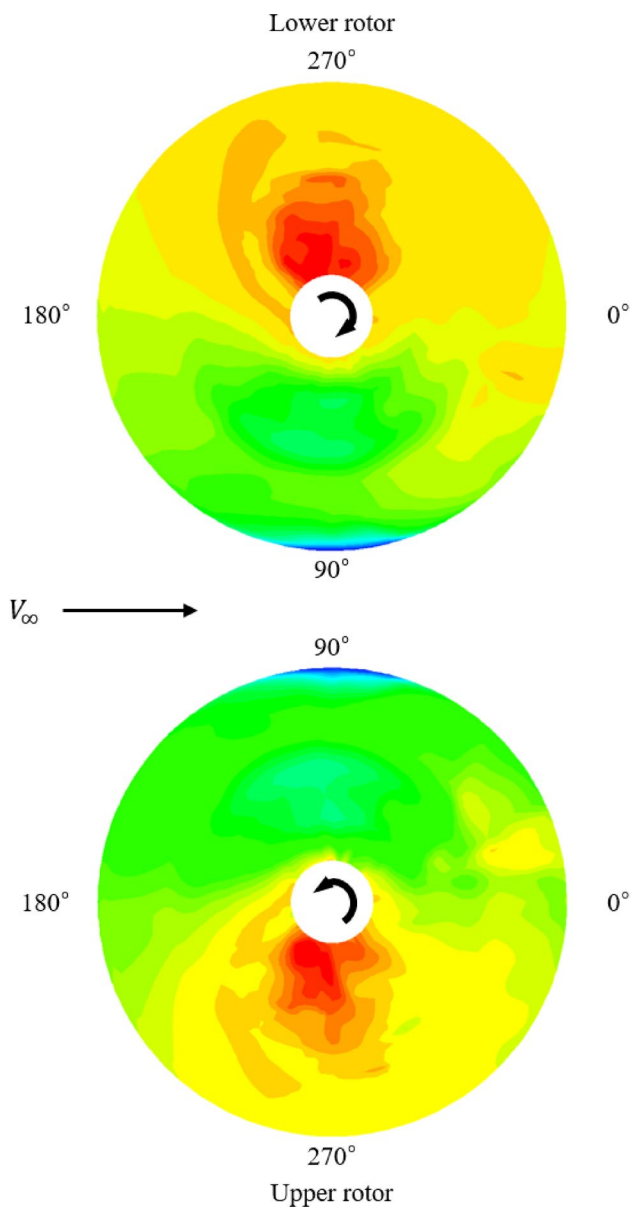
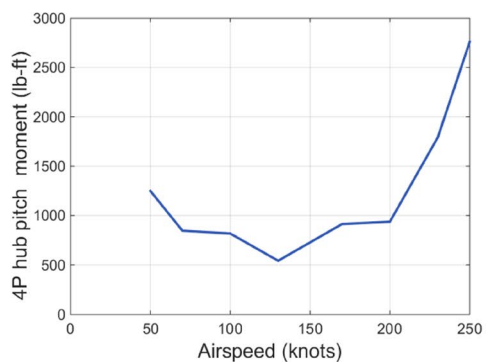
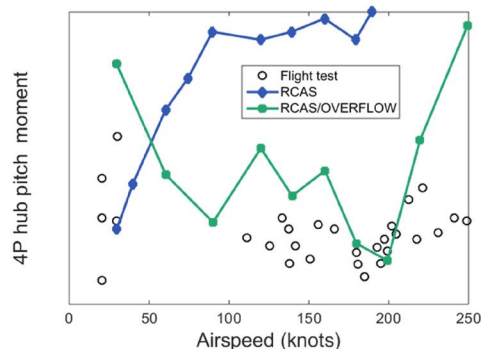


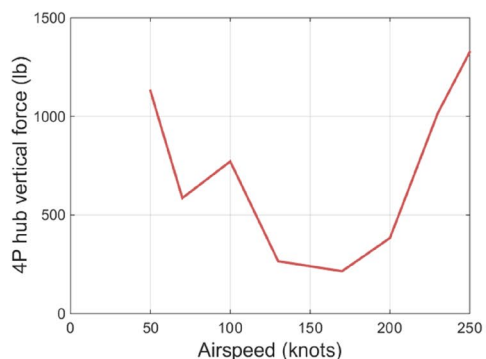
Fig. 18 Rotor pitching moment ($M^2 C_m$) distributions ($V=250$ knots)



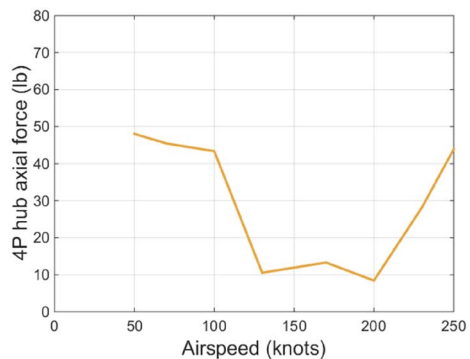
(a) Hub pitch moment



(b) Hub pitch moment [19]



(c) Hub vertical force



(d) Hub axial force

Fig. 19 The 4/rev hub vibratory load components. **a** Hub pitch moment, **b** Hub pitch moment [19], **c** Hub vertical force, and **d** Hub axial force

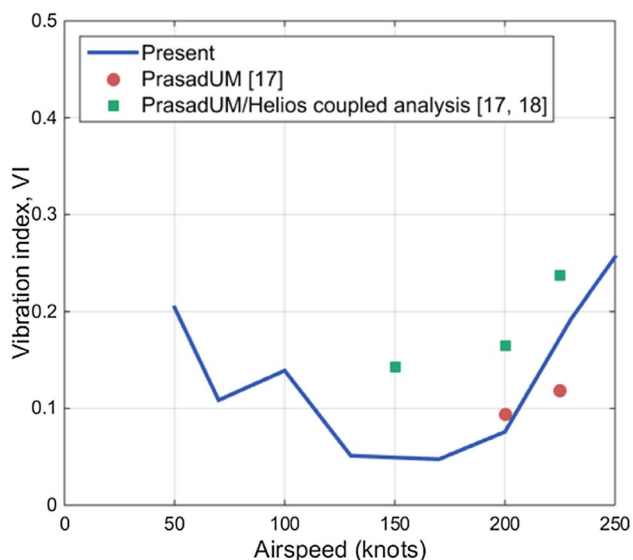


Fig. 20 Rotor vibration index

the freewake model [17]; however, it is underpredicted than the results by PrasadUM/Helios-coupled analysis [17, 18].

4 Conclusions

This study investigated the aeromechanics of the X2TD rotor, which is a modern lift-offset coaxial rotor. A rotorcraft comprehensive analysis code, CAMRAD II, was used for modeling and analyses of performance, blade airloads, and 4/rev hub vibratory loads of the X2TD rotor at flight speeds of up to 250 knots. The general freewake model was applied to represent the aerodynamic interactions between the upper and lower rotors. The natural frequencies of a rotating blade in the first flap, lead-lag, and torsion modes were compared well with the previous result, and the second flap mode frequency was validated moderately. However, the blade natural frequencies in the third flap and second lead-lag modes were unsatisfactorily predicted. Rotor performance, such as power and effective lift-to-drag ratio, was correlated excellently with the flight test data and previous analysis. In both the present analysis and flight test, the rotor power decreased with an increase in the flight speed; however, the power of the pusher propeller increased significantly to overcome the drag of a vehicle in high-speed flight. In the section airload analyses of the X2TD rotor blade at 250 knots, the impulses of the section lift forces (M^2C_l) of each rotor were observed because of the aerodynamic interactions between the upper and lower rotors, and the retreating blades of both rotors were off-loaded because of the unique characteristics of a lift-offset coaxial rotor. The 4/rev hub vibratory loads were investigated, and the variation trend of the present 4/rev hub

pitch moment was reasonably compared with the previous analysis result. In addition, the rotor vibration level (vibration index) increased significantly in high-speed flight, and it was compared well with the previous rotorcraft comprehensive analysis with the freewake model. Through this study, it was considered that the present modeling and analysis techniques were appropriate for the aeromechanics analyses of a modern lift-offset coaxial rotor.

Acknowledgements This work was supported by research fund of Chungnam National University.

References

- Ruddell AJ (1981) Advancing blade concept (ABC) technology demonstrator. US Army Research and Technology Laboratories, USAAVRADCOM-TR-81-D-5
- Bagai A (2008) Aerodynamic design of the X2 technology demonstrator™ main rotor blades. In: 64th American Helicopter Society International Annual Forum
- Anonymous (2005) Sikorsky to showcase coaxial rotor technology. Aviation Week and Space Technology, p.18
- Blackwell R, Millott T (2008) Dynamics design characteristics of the Sikorsky X2 technology™ demonstrator aircraft. In: 64th American Helicopter Society International Annual Forum
- Walsh D, Weiner S, Arifian K, Bagai A, Lawrence T, Blackwell R (2009) Development testing of the Sikorsky X2 technology™ demonstrator. In: 65th American Helicopter Society International Annual Forum
- Walsh D, Weiner S, Arifian K, Lawrence T, Wilson M, Millott T, Blackwell R (2011) High airspeed testing of the Sikorsky X2 technology™ demonstrator. In: 67th American Helicopter Society International Annual Forum
- Eller E (2012) X2™ load alleviating controls. In: 68th American Helicopter Society International Annual Forum
- Johnson W (2012) CAMRAD II: Comprehensive analytical method of rotorcraft aerodynamics and dynamics. Johnson Aeronautics
- Johnson W (2011) Lift-offset compound design background, X2TD, JMR ME1A status and plans. Aeromechanics Branch, NASA Ames Research Center.
- Johnson W, Moodie AM, Yeo H (2012) Design and performance of lift-offset rotorcraft for short-haul missions. In: the American Helicopter Society Future Vertical Lift Aircraft Design Conference
- Go JI, Kim DH, Park JS (2017) Performance and vibration analyses of lift-offset helicopters. Int J Aerosp Eng, Vol. 2017, Article ID 1865751
- Saberi HA, Khoshlahjeh M, Ormiston RA, Rutkowski MJ (2004) RCAS overview and application to advanced rotorcraft problems. In: 4th Decennial American Helicopter Society Aeromechanics Specialists' Conference
- Jacobellis G, Gandhi F, Floros M (2015) A physics-based approach to trim optimization of coaxial helicopters in high-speed flight. In: 71st American Helicopter Society International Annual Forum
- Jacobellis G, Gandhi F (2016) Investigation of performance, loads, and vibrations of coaxial helicopter in high speed-flight. In: 72nd American Helicopter Society International Annual Forum

15. Jacobellis G, Anusonti-Inthra P, Gandhi F (2018) Investigation of blade loads on a modern high-speed lift-offset coaxial helicopter using coupled computational fluid dynamics/computational structural dynamics. In: the American Helicopter Society International Aeromechanics Specialists' Meeting
16. Passe B, Sridharan A, Baeder J (2015) Computational investigation of coaxial rotor interactional aerodynamics in steady forward flight. In: 33rd AIAA Applied Aerodynamics Conference
17. Klimchenko V, Sridharan A, Baeder J (2017) CFD/CSD study of the aerodynamic interactions of a coaxial rotor in high-speed forward flight. In: 35th AIAA applied Aerodynamics Conference
18. Klimchenko V, Baeder J (2020) CFD/CSD study of interactional aerodynamics of a coaxial compound helicopter in high-speed forward flight. In: AIAA SciTech 2020 Forum
19. Tuozzo N, Fox E, Eller E, Mayrides B, Zientek TA, Lorber P, Narducci RP, Sproul T (2017) Analytic tool correlation status for the Joint Multi-Role technology demonstrator program. In: 73rd Annual American Helicopter Society International Forum and Technology Display
20. UIUC airfoil coordinates database. https://m-selig.ae.illinois.edu/ads/coord_database.html. Accessed 1 Apr 2019
21. Drela M (1996) A user's guide to MSES 2.95. MIT Computational Aerospace Science Laboratory
22. Leishman JG (2006) Principles of helicopter aerodynamics, 2nd edn. Cambridge University Press, Cambridge, pp 407–408
23. Yamauchi GK, Johnson W (1983) Trends of Reynolds number effects on two-dimensional airfoil characteristics for helicopter rotor analyses. NASA TM 84363
24. Lim JW (2016) Consideration of structural constraints in passive rotor blade design for improved performance. *Aeronaut J* 120(1232):1604–1631
25. O'Leary J, Miao W (1982) Design of higher harmonic control for the ABCTM. *J Am Helicopter Soc* 27(1):52–57

Publisher's Note Springer Nature remains neutral with regard to jurisdictional claims in published maps and institutional affiliations.